J. Synchrotron Rad. (1998). **5**, 596–599

Characterization of windows and filters for coherent X-ray beamlines

Yoshio Suzuki,[a]*† Atsushi Momose[a] and Hiroshi Sugiyama[b]

[a]Advanced Research Laboratory, Hitachi Ltd, Hatoyama, Saitama 350-03, Japan, and [b]Photon Factory, KEK, Tsukuba, Ibaraki, 305, Japan. E-mail: suzuki@harl.hitachi.co.jp

(*Received 4 August 1997; accepted 22 December 1997*)

Beryllium windows and graphite heat absorbers used in coherent X-ray beamlines must be optically flat. If the optical path through the window varies by more than λ/4, the X-ray wave front will be distorted after passing through the window, and the divergence of the X-ray beam may be increased. This reduces the beam coherence. Beryllium, graphite and Kapton films have been tested using ultra-small-angle X-ray scattering. Wave-front distortion was also directly observed by means of phase-contrast X-ray microradiography. The measured increase of angular divergence is about 4 μrad. The wave-front distortion is larger than 2π (optical path difference of λ). These are serious problems for utilizing coherent X-ray beams.

Keywords: coherence; X-ray beamlines; beryllium window; small-angle scattering; phase contrast.

1. Introduction

Beryllium foils are usually used as vacuum windows in hard X-ray synchrotron radiation beamlines. Graphite foils are used as heat absorbers in high-flux beamlines. Thin polymer films, *e.g.* Kapton, are also sometimes used as He/air windows. Important characteristics of these window and filter materials are high X-ray transmittance and mechanical toughness. Relatively little attention has been paid to the quality of the windows from the point of view of coherent optics, except for the evaluation of beryllium windows by means of Gabor-type holography (Snigirev *et al.*, 1996).

Coherent optics is considered to be one of the important applications at the third-generation synchrotron radiation light sources. The angular spread of an X-ray beam ($\Delta\theta$) observed at an experimental station is expressed as $\Delta\theta \simeq A/L$, where A is the transverse source size and L is the distance from the source to the observation point. In third-generation synchrotron radiation sources, the typical source size is $A \simeq 0.1$ mm, and L is around 50 m. Therefore, $\Delta\theta$ is about 2 μrad (∼0.4 arcsec). These highly collimated coherent beams are, for example, well suited to diffraction-limited microfocusing. However, X-ray beam transportation through the beamline is sometimes a very serious problem. All the optical components of the beamline must have sufficient accuracy for conserving the spatial and temporal coherence of the X-rays.

Undesirable wave-front distortions may be caused by passing through windows and filters having uneven surfaces, as shown in Fig. 1. Increase of the angular divergence of the X-ray beam may also occur due to the distortion of the wave-front. From the point of view of wave optics, it is well known that distortion of the wave-front should be smaller than $\pi/2$ (= λ/4 in optical path difference) for diffraction-limited focusing (Rayleigh quarter-wavelength rule). From the point of view of geometrical optics, the angular divergence caused by wave-front distortion should be smaller than the angular spread of the source ($\Delta\theta$) for conserving the transverse coherence of the light source. When the optical components (Be windows, filters, monochromator *etc.*) do not fulfil the above conditions, the X-ray wave front may be distorted by transportation through the beamline. The distortion of the wave front causes an angular spread of the transmitted beams.

When the window material is uniform in density, the relation between wave front distortion and unevenness of the window may be estimated by

$$\Delta\varphi = 2\pi\delta\,\Delta t/\lambda,$$

where $\Delta\varphi$ is the phase difference of the wave front, δ (= $1 - n$) is the difference of refractive index between the window material and a vacuum, and Δt is the window thickness error (surface roughness). Assuming the free-electron approximation and $Z/A \simeq 0.5$ (where Z is the atomic number and A is the atomic weight), δ is expressed by the well known formula (Parrat & Hempstead, 1954)

$$\delta \simeq 1.3 \times 10^{-6}\rho\lambda^2,$$

where ρ (g cm^{-3}) is the density of the window material, and λ (Å) is the X-ray wavelength. An example of the measured surface roughness of a beryllium foil is shown in Fig. 1. The roughness of the Be foil is about 9 μm peak-to-valley (p–v). Considering both sides of one foil, Δt is estimated to be about 18 μm. Therefore, assuming λ = 1 Å and ρ = 1.85 (metallic beryllium), $\Delta\varphi$ is about 0.8π. This value is larger than the optical path difference of λ/4. The distortion of the wavefront caused by the X-ray windows cannot be neglected.

Characterization of the window materials has already been performed by Henderson (1995) for the purpose of small-angle-scattering experiments. However, the measured scattering angle was limited to larger than 1 mrad at 1.54 Å. Small-angle-scattering measurements with higher angular resolution are needed to discuss the conservation of coherence. Cloetens *et al.* (1996) have characterized the angular broadening caused by 'random phase plates' using the same method as that used in our experiment. However, the angular resolution was about 50 μrad at λ = 0.7 Å. This angular resolution was insufficient to evaluate the beryllium windows and graphite filters.

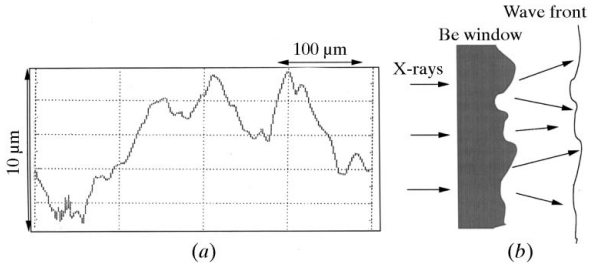

Figure 1
(*a*) Surface figure of typical beryllium foil (type #1) and (*b*) schematic diagram of wave-front distortion and angular spread of transmitted X-rays due to surface roughness.

† Present address: Japan Synchrotron Radiation Research Institute, SPring-8, Kamigori, Hyogo 678-12, Japan.

It is necessary to characterize the X-ray window/filter materials in terms of conservation of coherence. This paper describes quantitative characterization of these materials, using ultra-small-angle X-ray scattering and phase-contrast X-ray microradiography with an X-ray interferometer.

2. Samples and experimental set-up

Distortion of a wave front can be evaluated quantitatively by two methods: one is measurement of the angular distribution of an X-ray beam transmitted through the window, *i.e.* a kind of small-angle-scattering measurement, and the other is phase-contrast X-ray microradiography.

The experiments were performed at the experimental station BL-8C2 of the 2.5 GeV storage ring in the Photon Factory, KEK. As shown in Fig. 2, we use a Bonse–Hart type ultra-small-angle-scattering measurement system (Bonse & Hart, 1966) to measure the small-angle scattering of the X-ray beam through the windows/filters. The experimental set-up is basically the same as that of previous work (Uchida & Suzuki, 1992). Synchrotron radiation is monochromated and collimated with an Si 440 channel-cut monochromator, and incident to the specimen. The X-ray beam through the specimen is analysed by an Si 440 crystal. The plane of incidence is set in the horizontal direction to use the π component of synchrotron radiation.

We also use a phase-contrast X-ray computed-tomography measurement system developed by Momose (Momose, 1995; Momose *et al.*, 1998) to measure the X-ray phase-contrast image. The instrument (see Fig. 3) consists of a Laue-Laue-Laue interferometer (Bonse & Hart, 1965) and an interference-fringe-scanning system with rotatable-plate phase shifter for quantitative two-dimensional phase-difference mapping. The phase distribution of the X-ray beam, $\varphi(x)$, emerging from the window is connected to the angular distribution $F(k_x)$ by a Fourier transformation (Mandel & Wolf, 1995),

$$F(k_x) = \int \varphi(x) \exp(-k_x x)\, \mathrm{d}x,$$

where x is the coordinate on the sample surface perpendicular to the incident X-ray beam, and k_x is the x component of the wavevector of the scattered wave. k_x is expressed as,

$$k_x = k_0 \sin\theta,$$

where $k_0 = 2\pi/\lambda$, and θ is the scattering angle, which is related to the spatial period Δx by

$$\sin\theta = \lambda/\Delta x.$$

Therefore, if the angular resolution is infinitely small, we need not measure the phase image. However, in our experiment, the angular resolution is about 4 μrad at λ = 1.54 Å. This value corresponds to the spatial period of 40 μm. On the other hand, the spatial resolution in phase-contrast radiography is estimated to be less than 40 μm, but not better than 10 μm. Therefore, in this experiment, these two methods give complementary information because of the insufficient angular resolution and lack of spatial resolution.

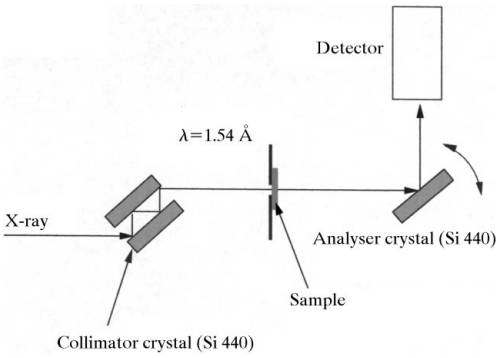

Figure 2
Experimental set-up for ultra-small-angle-scattering measurements (Bonse–Hart small-angle camera). The cross section of the X-ray beam incident to the sample is 0.2 mm × 0.2 mm.

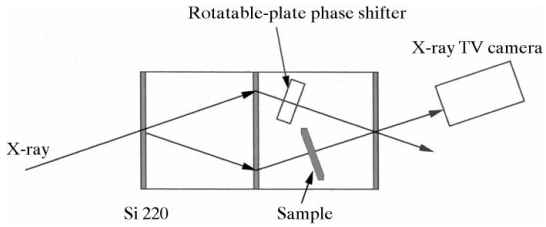

Figure 3
Experimental setup for phase-contrast microradiography (Laue-Laue-Laue interferometer with rotatable-plate phase shifter).

Table 1
List of samples.

Material	Thickness	Surface roughness (peak-to-valley)
Be metal #1	0.2 mm	8.9 μm
Be metal #2†	0.2 mm	1.1 μm
Kapton	0.05 mm	0.03 μm
Graphite	0.1 mm	1.0 μm

† Roughness of this Be foil is specified as JIS-3.2S.

Two kinds of Be windows were tested: one was supplied by NGK Corporation, Japan (Be #1), the other was of IF-1-grade Be foil purchased from Brush–Wellman Inc., USA (Be #2). Be #1 is the type widely used at the Photon Factory beamlines as a vacuum window. Be #2 was used in the Tristan main-ring test beamline (Sugiyama *et al.*, 1997; Suzuki *et al.*, 1997). The graphite foil was the same as that used in the Tristan main-ring test beamline.

The surface roughness is measured with needle contact apparatus. As shown in Table 1, Be #1 has a roughness of 8.9 μm p-v. Be #2 is relatively flat (1.1 μm p-v). The Kapton film is optically flat

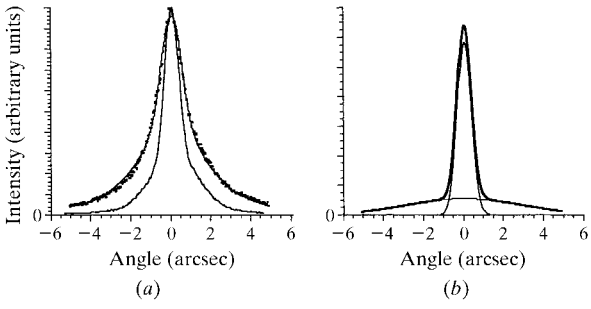

Figure 4
Small-angle scattering of the X-ray beam passing through the window and filter. (*a*) Dots represent measured data. The sample is a combination of three Be #2 foils, two graphite foils and four Kapton films. The measured instrumental function is shown by the lower line, and the result of the least-squares curve fitting is shown by the other line. (*b*) Result of deconvolution from the measured instrumental function. The thinner lines represent the narrow and broad components.

Table 2
Results of least-squares fitting for angular broadening.

Sample	a_1	σ_1 (arcsec)	a_2	σ_2 (arcsec)	FWHM (arcsec)
Be (BW) × 3 + Graphite × 2 + Kapton × 4	1.164	0.3600	0.111	2.864	0.91 (4.4 μrad)
Be (NGK) × 3	2.498	0.1661	0.015	1.469	0.40 (1.9 μrad)
Be (BW) × 3	4.926	0.0762	0.042	2.506	0.18 (0.9 μrad)
Kapton × 6†	–	–	–	–	–
Graphite × 2	1.270	0.3494	0.068	3.079	0.85 (4.1 μrad)

† The measured profile for Kapton films agrees with the instrumental function.

(0.03 μm p-v). The graphite foil seems to have a fairly smooth surface (1.0 μm p-v).

3. Results and discussions

Results of the ultra-small-angle-scattering measurements for a typical combination of windows/filters and the instrumental resolution are shown in Fig. 4(*a*). The sample is a combination of two graphite filters, three Be foils (type #2) and four Kapton films, which is the same as that used in the Tristan main-ring test beamline. The measured angular broadening is about 2 arcsec full width at half-maximum (FWHM) at a wavelength of 1.54 Å. This angular broadening is larger than the instrumental resolution (0.9 arcsec in FWHM). However, the instrumental resolution is not negligibly small so as to derive intrinsic broadening. We estimate the intrinsic angular divergence by deconvoluting the measured small-angle scattering with the measured instrumental function. The measured profiles are considered to consist of strong sharp peaks and weak broad scattering tails. Therefore, for this purpose, Gaussian-type broadening is assumed as

$$f(\theta) = a_1 \exp(-\theta^2/2\sigma_1^2) + a_2 \exp(-\theta^2/2\sigma_2^2),$$

and a least-squares fitting is adapted. The first term corresponds to the 'strong narrow peak' and the second term represents the 'broad weak tail'. The result of the least-squares fitting is shown in Fig. 4(*b*). The angular divergence of the X-ray beam through the windows and filters is 0.91 arcsec (∼4.4 μrad) FWHM, and a broad weak tail is also observed. This angular broadening is not negligible for coherent X-ray optics. Although the origin of the angular broadening is not clear yet, we think that the narrow peak is caused by surface undulation or large porosity and its spatial period is around several tens of μm. The broad tail seems to be due to grain boundaries or other fine structures, and the spatial period is estimated to be a few μm.

Each component of the windows and filters is investigated to evaluate which component gives the significant effect to angular broadening. Results for Be #1, Be #2, Kapton and graphite films are shown in Figs. 5(*a*)–5(*d*). The instrumental broadening is removed from the measured small-angle-scattering profiles in a similar manner. Results of the least-squares curve fitting are listed in Table 2. The results for Kapton are not shown in the table because the measured angular distribution for Kapton film agrees with the instrumental function within experimental error. Therefore, the Kapton foil is considered to be an optically flat window for hard X-rays. On the contrary, the graphite foil shows the most significant angular broadening of 0.85 arcsec.

Results of phase-contrast imaging of the test samples are shown in Fig. 6; one-dimensional phase-difference profiles are also shown in the figure. The phase-contrast images are taken at an X-ray wavelength of 0.92 Å. All the images are displayed as grey scale of

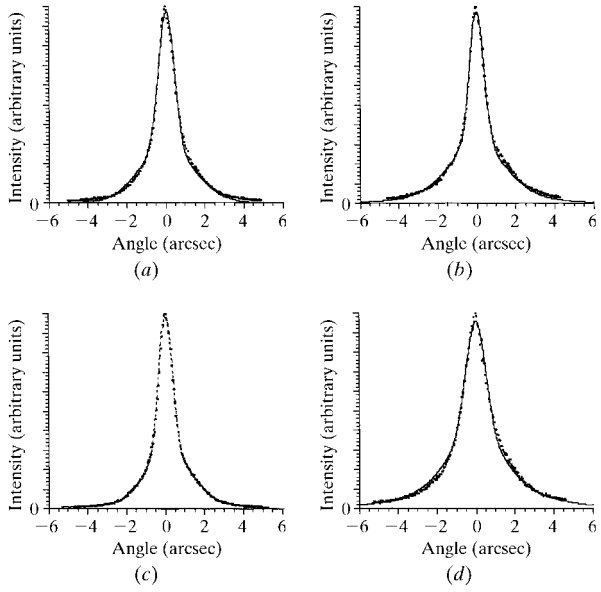

Figure 5
Small-angle scattering of the X-ray beam passing through various windows and filters. (*a*) Three Be foils (NGK), (*b*) three Be foils (Brush–Wellman), (*c*) six Kapton films, (*d*) two graphite foils. Dots are measured data, and fits are shown by solid lines in (*a*), (*b*) and (*d*). The dashed line in (*c*) is the measured instrumental function.

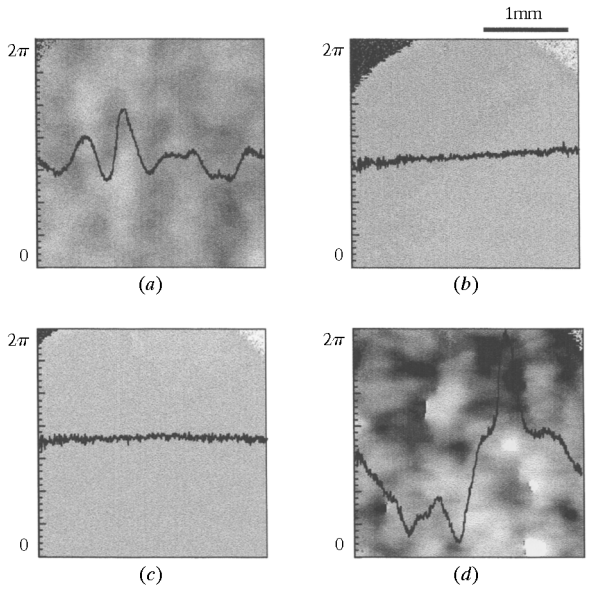

Figure 6
Two-dimensional phase images measured with an X-ray interferometer. (*a*) Be #1 foil (NGK), (*b*) Be #2 foil (Brush–Wellman), (*c*) Kapton film, (*d*) graphite film. One-dimensional phase-difference profiles extracted from the two-dimensional mapping are shown on the phase images.

2π. Although no significant non-uniformities are observed in Be #2 and Kapton foils within experimental errors, the graphite foil shows a phase difference of about 2π p-v, and the Be #1 foil shows a phase perturbation of about 0.7π p-v.

Peak-to-valley values of phase difference for the Be foils and Kapton film can be explained by the surface figure profiles. Therefore, the phase distortion is considered to be caused mainly by the figure errors (surface roughness) of the films. On the contrary, the graphite foil shows significant wave-front distortion of about 2π in spite of its almost flat surface. It is suggested that this large phase distortion and broad angular divergence may be caused by the porosity of the graphite. Therefore, optical components in coherent optics beamlines cannot be checked only by measurement of surface figures; it is important to investigate them by means of the interferometric method, holography or phase-contrast microscopy, and by means of ultra-small-angle-scattering measurements.

References

Bonse, U. & Hart, M. (1965). *Appl. Phys. Lett.* **6**, 155–156.

Bonse, U. & Hart, M. (1966). *Z. Phys.* **189**, 151–162.

Cloetens, P., Barrett, R., Baruchel, J., Guigay, J. & Shlenker, M. (1996). *J. Phys. D*, **29**, 133–146.

Henderson, S. (1995). *J. Appl. Cryst.* **28**, 820–826.

Mandel, L. & Wolf, E. (1995). *Optical Coherence and Quantum Optics.* Cambridge University Press.

Momose, A. (1995). *Nucl. Instrum. Methods*, A**352**, 622–628.

Momose, A., Takeda, T., Itai, Y., Yoneyama, A. & Hirano, K. (1998). *J. Synchrotron Rad.* **5**, 309–314.

Parrat, L. G. & Hempstead, C. F. (1954). *Phys. Rev.* **94**, 1593.

Snigirev, A., Snigireva, I., Kohn, I. V. & Kuznetsov, S. M. (1996). *Nucl. Instrum. Methods*, A**370**, 634–640.

Sugiyama, H., Zhang, X., Higashi, Y., Arakawa, E. & Ando, M. (1997). To be published.

Suzuki, Y., Kamijo, N., Tamura, S., Handa, K., Takeuchi, A., Yamamoto, S., Sugiyama, H., Ohsumi, K. & Ando, M. (1997). *J. Synchrotron Rad.* **4**, 60–63.

Uchida, F. & Suzuki, Y. (1992). *Proc. SPIE*, **1720**, 264–271.